Development 139, 3422-3431 (2012) doi:10.1242/dev.083154

Pten deletion causes mTorc1-dependent ectopic neuroblast differentiation without causing uniform migration defects

Guo Zhu[1,2], Lionel M. L. Chow[1,*], Ildar T. Bayazitov[1], Yiai Tong[1], Richard J. Gilbertson[1], Stanislav S. Zakharenko[1], David J. Solecki[1] and Suzanne J. Baker[1,2,‡]

SUMMARY

Neuronal precursors, generated throughout life in the subventricular zone, migrate through the rostral migratory stream to the olfactory bulb where they differentiate into interneurons. We found that the PI3K-Akt-mTorc1 pathway is selectively inactivated in migrating neuroblasts in the subventricular zone and rostral migratory stream, and activated when these cells reach the olfactory bulb. Postnatal deletion of *Pten* caused aberrant activation of the PI3K-Akt-mTorc1 pathway and an enlarged subventricular zone and rostral migratory stream. This expansion was caused by premature termination of migration and differentiation of neuroblasts and was rescued by inhibition of mTorc1. This phenotype is reminiscent of lamination defects caused by *Pten* deletion in developing brain that were previously described as defective migration. However, live imaging in acute slices showed that *Pten* deletion did not cause a uniform defect in the mechanics of directional neuroblast migration. Instead, a subpopulation of Pten-null neuroblasts showed minimal movement and altered morphology associated with differentiation, whereas the remainder showed unimpeded directional migration towards the olfactory bulb. Therefore, migration defects of Pten-null neurons might be secondary to ectopic differentiation.

KEY WORDS: Pten, Differentiation, Migration, Neuroblast, mTOR/PI3K, Mouse

INTRODUCTION

In rodent brain, thousands of new neuronal precursors are born every day in the subventricular zone (SVZ), the postnatal neural stem cell niche in the lateral walls of the lateral ventricles. Multiple cell types reside in this niche including 'type B' Gfap-expressing neural stem cells that generate 'type C' Mash1 (Ascl1 – Mouse Genome Informatics)-expressing transit-amplifying cells. Transit-amplifying cells further differentiate into 'type A' migrating neuronal precursor cells or neuroblasts that express the microtubule-associated protein doublecortin (Dcx). Neuroblasts migrate from the SVZ through the rostral migratory stream (RMS) to the olfactory bulb (OB) where they differentiate into interneurons and are integrated into local circuits (Alvarez-Buylla and Garcia-Verdugo, 2002).

In contrast to much of embryonic development in which immature neurons migrate along radial glial fibers, in the RMS, neuroblasts migrate along one another in a chain formation, separated from the surrounding brain parenchyma by a glial tube (Ghashghaei et al., 2007). Removal of the OB does not disrupt this rostral migration, indicating that long-distance chemoattractant signals emanating from the final destination are not required (Kirschenbaum et al., 1999). Chemorepulsive cues involving secreted SLIT ligands and their receptors, the ROBO family of proteins, are involved in directing newly generated neuroblasts to enter the RMS from the SVZ, and in mediating interactions in the RMS between migrating neuroblasts and astrocytes that form the glial tube. Extracellular matrix cues, including polysialated neuronal cell adhesion molecule (PSA-NCAM) and integrin signaling, are also important for normal migration through the RMS to the OB, and reelin and tenascin R act as a detachment signal to dictate the switch from tangential to radial migration when neuroblasts reach the OB (Ghashghaei et al., 2007). Additional guidance cues might be provided by the vasculature along the RMS (Snapyan et al., 2009). Thus, diverse extracellular cues dictate the continual process of directional migration of neuroblasts from the SVZ through the RMS to their final destination as integrated interneurons in the OB. However, the intracellular signaling pathways that respond to these extracellular cues, instructing when and where migrating neuroblasts stop, are largely unknown.

The phosphoinositide 3-kinase (PI3K) signaling pathway is an evolutionarily conserved intracellular signaling cascade that transduces extracellular signals to regulate multiple processes, including proliferation, survival, metabolism and cell migration (Engelman et al., 2006). PI3Ks phosphorylate phosphatidylinositol-4,5-bisphosphate (PIP2) to generate phosphatidylinositol-3,4,5-trisphosphate (PIP3), resulting in downstream consequences, including activation of the serine-threonine kinase Akt, suppression of the tuberous sclerosis complex, and activation of mTorc1 (mTOR complex 1). Pten is the major negative regulator of the PI3K pathway, acting as a lipid phosphatase to directly antagonize PI3K by dephosphorylating PIP3 to PIP2 (Chalhoub and Baker, 2009).

Through numerous studies employing different cell types, the PI3K pathway has been shown to influence cell migration at multiple levels, including transducing chemotactic signals, establishing cell polarity and influencing cell adhesion (Cain and Ridley, 2009). In *Dictyostelium*, PTEN was required for directional migration towards a chemotactic stimulus (Funamoto et al., 2002; Iijima and Devreotes, 2002). However, more recently *Dictyostelium* simultaneously lacking all Class I PI3K isoforms and PTEN were shown to have normal directional chemotactic migration, but reduced speed. The most substantial effect of PTEN

[1]Department of Developmental Neurobiology, St Jude Children's Research Hospital, Memphis, TN 38105, USA. [2]Integrated Program in Biomedical Sciences, The University of Tennessee Health Science Center, Memphis, TN 38105, USA.

*Present address: Division of Oncology, Cincinnati Children's Hospital Medical Center, Cincinnati, OH 45229, USA
‡Author for correspondence (Suzanne.Baker@StJude.org)

Accepted 25 June 2012

deletion in this study was a decrease in random movement in the absence of a chemotactic signal (Hoeller and Kay, 2007). Thus, even within simple organisms, the precise mechanisms through which PI3K signaling influences migration are not straightforward.

Inherited mutations disrupting PI3K-AKT-mTORC1 regulation are associated with human syndromes that include neurological abnormalities, indicating that the pathway is important in normal neural development and/or function (Inoki et al., 2005; Endersby and Baker, 2008). Conditional knockout mice showed that Pten is important in brain for diverse processes, including proper neuronal positioning during development as well as negative regulation of neural stem cell self-renewal and proliferation, and neuronal morphogenesis and size regulation (Backman et al., 2001; Kwon et al., 2001; Marino et al., 2002; Waite and Eickholt, 2010). However, the underlying mechanism of how Pten is involved in neuronal migration is currently unknown.

In the present study, we demonstrated that Pten inhibits downstream activation of mTorc1 in normal migrating neuroblasts in the RMS. Postnatal deletion of Pten in this population resulted in ectopic positioning of neurons that failed to reach their final destination, reminiscent of defects in radial glia-guided neuronal migration caused by Pten deletion during development. The phenotype was fully rescued by rapamycin, demonstrating that mTorc1 is required for the Pten-mediated regulation of migration in the RMS. We used live imaging of slice cultures to visualize the defect in migrating neurons. Unlike the more uniform phenotypes induced throughout the population in PTEN-deficient *Dictyostelium*, we found that a subpopulation of Pten-null neuroblasts showed normal directional migration, whereas another subpopulation showed a complete lack of directional migration and showed non-polarized morphology. This altered morphology was associated with the expression of markers of differentiation. This strongly suggests that the neuroblast migration defect associated with Pten loss might be secondary to precocious differentiation rather than a defect in the mechanics of directional migration in the RMS.

MATERIALS AND METHODS

Mice

Nestin-creER^{T2} mice (Cicero et al., 2009) contain a transgene comprising the *Nestin* promoter and second intron (Zimmerman et al., 1994) driving expression of CreER^{T2} (Metzger et al., 1995; Feil et al., 1996; Feil et al., 1997), an internal ribosomal entry site (IRES) and human placental alkaline phosphatase (hPLAP; ALPP – Human Gene Nomenclature Database) specifically in progenitor cells in the central nervous system. To map Cre activity, *Nestin-creER^{T2}* transgenic mice were bred with the *R26R-lacZ* reporter (R26R) (Soriano, 1999) or *R26LSL-EYFP* (Srinivas et al., 2001) mice to generate *Nestin-creER^{T2};R26R-lacZ* or *Nestin-creER^{T2};R26LSL-EYFP* mice. To generate *Pten^{cKO}* mice (*Nestin-creER^{T2}; Pten$^{loxP/loxP}$* or *R26LSL-EYFP;Pten$^{loxP/loxP}$* for *cre* electroporation experiments), *Pten^{loxP}* mice (Suzuki et al., 2001) were intercrossed with *Nestin-creER^{T2}* or *R26LSL-EYFP* mice. For all analyses including *Nestin-creER^{T2}*, the transgene was hemizygous to avoid variation from transgene dosage. Controls were littermate *Pten$^{loxP/loxP}$* mice without *Nestin-creER^{T2}*. All procedures were reviewed and approved by the Animal Care and Use Committee at St Jude Children's Research Hospital.

Cre induction

Tamoxifen (TM; Sigma) was dissolved at 20 mg/ml or 5 mg/ml at 37°C in corn oil (Sigma) for Cre induction in adult mice or pups, respectively, filter sterilized and stored at 4°C in the dark for up to 10 days. Cre activity was induced by intraperitoneal (i.p.) injection of TM at 3 mg/40 g body weight daily from postnatal day (P) 0 to P1, or from P11 to P12, as indicated, in pups, or 9 mg/40 g body weight daily from P28 to P30 in adults. Daily injections were separated by 24 hours. Sterile corn oil was the vehicle control.

5-Bromo-2′-deoxyuridine injection and rapamycin treatment

5-Bromo-2′-deoxyuridine (BrdU; Sigma) at 5 mg/ml in sterile PBS was stored at –20°C. BrdU (50 μg/g body weight) was injected i.p. five times at 2-hour intervals for short-term BrdU labeling, or six times at 12-hour intervals from P4 to P6 for BrdU birthdating.

Rapamycin (LC Laboratories) at 20 mg/ml in sterile dimethyl sulfoxide (DMSO) was stored at –20°C and diluted in 5.2% Tween80 immediately before use. Rapamycin (1.5 μg/g body weight) was injected i.p. daily from P8 to P31. Sterile DMSO+Tween80 was the vehicle control. When TM was given on the same day, the two drugs were separated by 6 hours.

Histochemistry, immunohistochemistry and immunofluorescence

For cryosections, mice were anesthetized and perfused transcardially with PBS followed by 2% paraformaldehyde (PFA) in PBS. Following dissection, tissues were post-fixed overnight in 2% PFA in PBS at 4°C, and then equilibrated in 25% sucrose in PBS for an additional 24 hours at 4°C. Tissues were embedded in TBS embedding media (Triangle Biomedical Sciences) on dry ice and cut into 12 μm-thick cryosections. Tissue slides were equilibrated at room temperature for 20 minutes then washed three times in PBS prior to staining. Cre reporter activity from the *R26R-lacZ* reporter was detected by X-gal staining to detect β-galactosidase activity (Chow et al., 2008). Cre reporter activity from *R26LSL-EYFP* mice was detected by anti-GFP immunofluorescence (IF) on cryosections.

For paraffin sections, tissue was processed the same way as above except using 4% PFA for perfusion and 24 hour post-fixation, then embedded in paraffin, and cut into 5 μm sections. Primary antibodies for immunostaining were: anti-GFP (1:1000, Invitrogen A6455; 1:2000, Abcam #13970), anti-Pten [1:100 for immunohistochemistry (IHC), 1:500 for IF with tyramide amplification, Cell Signaling #9559], anti-p-Akt S473 (1:50, Cell Signaling #9271), anti-p-S6 S235/236 (1:500, Cell Signaling #2211), anti-Dcx (1:4000 for IHC, 1:500 for IF, Chemicon AB5910), anti-Mash1 (1:100, BD #556604), anti-NeuN (1:500, Chemicon), anti-Map2 (1:5000, Sternberger SMI52), anti-calretinin (1:2000, Chemicon AB149), anti-tyrosine hydroxylase (1:500, Sigma T1299), anti-Gfap (1:200, Sigma G3893), anti-Ki67 (1:5000, Novocastra NCL-Ki67p), anti-BrdU (1:1000, AbDSerotec OBT0030CX) and anti-active Caspase3 (1:1000, BD #559565). All IHC used microwave antigen retrieval, biotinylated secondary antibodies in conjunction with horseradish peroxidase-conjugated streptavidin (Elite ABC, Vector Laboratories), color development with substrates NovaRed, DAB or VIP (Vector Laboratories) and counterstaining with Hematoxylin or Methyl Green (Vector Laboratories). For IF, AlexaFluor 488-, AlexaFluor 647- (Invitrogen) and Cy3-, Cy5- (Jackson ImmunoResearch) conjugated secondary antibodies were employed along with Vectashield mounting media containing 4′,6-diamidino-2-phenylindole (DAPI) (Vector Laboratories). A Tyramide Signal Amplification Kit (Perkin Elmer) was used for Pten and p-Akt S473 IF. All IF images are shown as *z*-stack projections from confocal microscopy. Terminal deoxynucleotidyl transferase-mediated nick end labeling (TUNEL) staining was conducted with the ApopTag Peroxidase In Situ Apoptosis Detection Kit (Chemicon, S7100).

Ki67 and BrdU quantification

Ki67 or BrdU IHC was quantitated from anatomically matched sections. For proliferation, the Bioquant system (R&M Biometrics) was used to count all Ki67+ cells in the SVZ. For BrdU birthdating (Fig. 6), BrdU+ cell number and granule cell density in a 20× objective field in the same areas of OB GCL or total number of BrdU+ cell in the SVZ were counted with ImageJ v1.44 cell counter. Four controls and four *Pten^{cKO}* brains were analyzed for each group and positive cells were counted from three sections from each brain for each staining. Two-tailed Student's *t*-test was used for statistical significance analysis.

In vivo electroporation

In vivo electroporation was performed similarly to previous reports (Boutin et al., 2008; Chesler et al., 2008). Endotoxin-free *pCAG-cre* expression plasmid (2 μl of 0.65 μg/μl, in PBS containing 1% Fast Green) was injected into the lateral ventricle of P2 pups with a 30G needle Hamilton syringe using the midpoint between Bregma and Lambda and 1 mm lateral to the midline suture as landmarks. Fast Green dye allowed visual

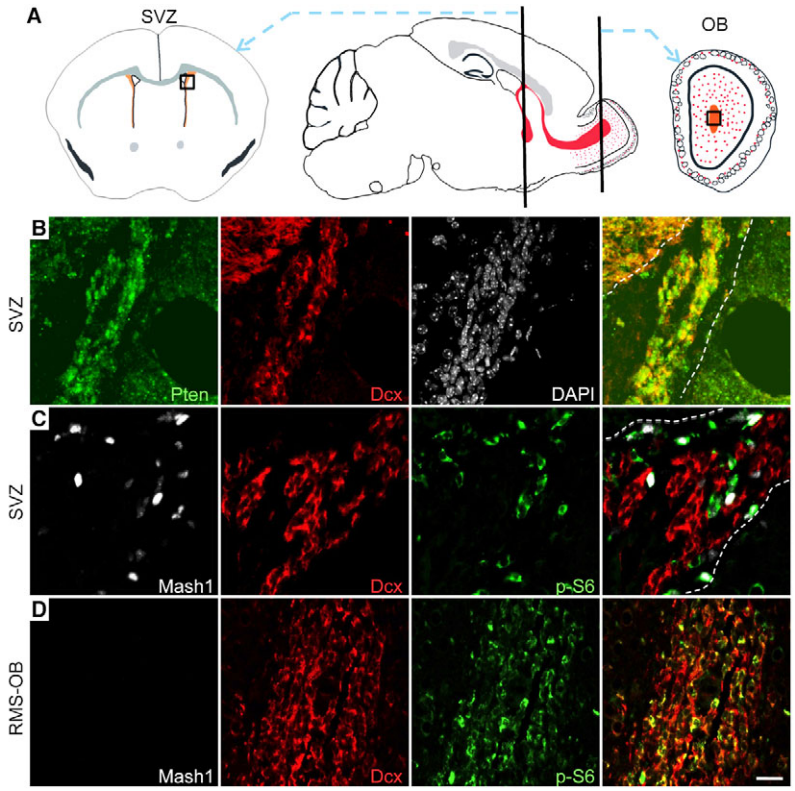

Fig. 1. The PI3K-mTorc1 pathway was inactive in migrating SVZ neuroblasts, but activated in OB neuroblasts. (**A**) Schematic brain sections indicating anatomical regions in the SVZ and OB (black boxes) from which images were captured. (**B-D**) IF staining of the SVZ (B,C) and the terminal RMS at the OB core (D) in coronal sections from 6-month-old (B,D) or 18-day-old (C) wild-type mice. (B) Pten (green) and Dcx (red) double IF labeling of the SVZ. Nuclei were labeled with DAPI (white). Pten was expressed in Dcx+ cells in the SVZ (overlay of Pten and Dcx, far right panel). (C,D) Mash1 (white), Dcx (red) and p-S6 (green) triple IF labeling of the SVZ (C) and OB (D) (overlay, far right panel). p-S6 was expressed in Mash1+ transit-amplifying cells but not Dcx+ neuroblasts in the SVZ (C), whereas in the OB, a substantial population of Dcx+ neuroblasts expressed p-S6 (D). The white dashed lines in the overlay mark the boundary of the SVZ in panels A and B. Scale bar: 20 μm.

confirmation of correct injection into lateral ventricles. Only successfully injected animals were subjected to five square-wave electrical pulses (50 mseconds separated by intervals of 950 mseconds, 150 V).

Brain slice preparation

Mouse brains were placed in sterile cold (4°C) dissecting Complete Hank's Balanced Salt Solution (complete HBSS) containing 1× HBSS (GIBCO), 2.5 mM Hepes (pH 7.4, GIBCO), 30 mM D-glucose, 1 mM $CaCl_2$, 1 mM $MgSO_4$ and 4 mM $NaCO_3$ (Polleux and Ghosh, 2002), dissected, embedded in 3% low-melting point agarose (Promega) and cut into 300 μm-thick sagittal sections with a vibratome. Slices containing the RMS were identified by enhanced yellow fluorescent protein (EYFP) expression, equilibrated for 2 hours in artificial cerebrospinal fluid (aCSF) containing 125 mM NaCl, 2.5 mM KCl, 2 mM $CaCl_2$, 2 mM $MgCl_2$, 1.25 mM NaH_2PO_4, 26 mM $NaHCO_3$ and 20 mM D-glucose (285-295 mOsm) with 95% O_2/5% CO_2 at room temperature and then transferred into the submerged recording chamber and superfused (1-2 ml/minute) with warm (36-37°C) aCSF.

Two-photon live imaging and migration analysis

Time-lapse live imaging was acquired by two-photon laser-scanning microscopy equipped with an Ultima imaging system (Prairie Technologies), a Ti:sapphire Chameleon Ultra femtosecond-pulsed laser (940 nm) (Coherent) and a 20× 0.95 numerical aperture water-immersion infrared objective (Olympus). *z*-stacks (512 × 512 pixels, 0.079 μm/pixel, 60-100 sections per stack, 1 μm/section) were collected at the elbow of the RMS every 5 minutes for 3-6 hours.

Maximum projections of 20 consecutive sections in the middle of *z*-stacks of time-lapse live imaging were analyzed using SlideBook v5.0 (Intelligent Imaging Innovations). Cells that exhibited bipolar morphology and moved at least two cell body lengths were counted as 'bipolar migrating cells'. All other cells were considered to be 'stationary or non-polar cells'. For each movie, all the EYFP+ cells were manually tracked but only those that could be observed more than ten consecutive frames (45 minutes) were included in the analysis. The average speeds (total displacement/time) or endpoint speeds (the distance between the first and last time points of the path/time) were binned in 20 μm/hour intervals to obtain a distribution. χ^2 analysis or Student's *t*-test was used to assess the significance of the distributions or means, respectively, of average speeds (or endpoint speeds).

RESULTS

PI3K pathway activity in the wild-type SVZ-RMS-OB

To understand PI3K signaling regulation in the SVZ-RMS-OB (Fig. 1A), we examined expression of several key components of the pathway. Levels of Pten expression were heterogeneous in the SVZ, and all of the cells expressing Pten were Dcx+ neuroblasts (Fig. 1B). In the SVZ and proximal RMS, the majority of cells expressing p-S6, a downstream indicator of PI3K-mTorc1 pathway activity, were Mash1+ transit-amplifying cells, and not Dcx+ migrating neuroblasts (Fig. 1C) (data not shown). By contrast, in the terminal RMS at the OB core, a substantial population of Dcx+ type A cells expressed p-S6 (Fig. 1D). This indicates that the PI3K pathway was not strongly active in migrating neuroblasts until these cells reached their destination in the OB.

Postnatal deletion of Pten caused ectopic differentiated neurons in an expanded SVZ and proximal RMS

To evaluate the function of the PI3K pathway regulator Pten in the postnatal neural stem/progenitors, we generated *Nestin-creER^{T2}* mice with inducible Cre activity in the SVZ (supplementary material Fig. S1) and bred them to *Pten$^{loxP/loxP}$* (Suzuki et al., 2001) to generate inducible *Pten* conditional knockout mice (hereafter *Pten^{cKO}*). Induction of *Pten* deletion in adult SVZ by tamoxifen (TM) injection in *Pten^{cKO}* mice at P30-32 did not cause obvious neurological abnormalities throughout a normal lifespan except for occasional seizures in some aged animals. Analysis of all *Pten^{cKO}* brains (*n*=24) showed dramatic expansion of the SVZ (Fig. 2A) and proximal

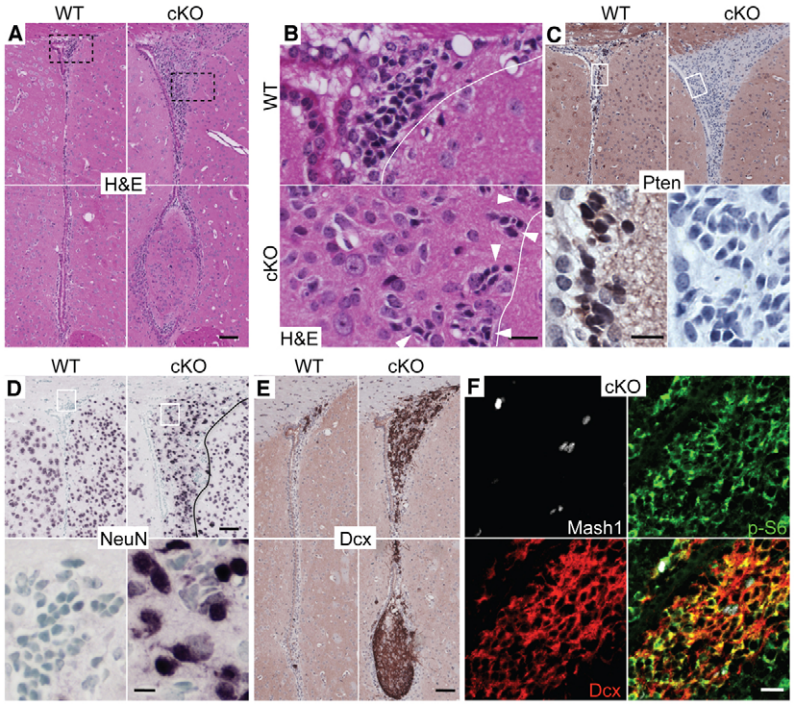

Fig. 2. Postnatal Pten deletion caused ectopic differentiated neurons in an expanded SVZ. Representative Hematoxylin & Eosin (H&E) (A,B), IHC (C-E) and IF (F) staining of the SVZ in matched coronal sections from mice injected with TM on P30-32 and analyzed more than 70 days later (*n*=24). A and E upper and lower panels show dorsal and ventral SVZ, respectively. (**A**) H&E staining showed that the *Pten*^{cKO} (cKO) SVZ was expanded compared with wild type (WT). (**B**) Higher magnification from WT (upper panel) and cKO (lower panel) shown in boxed areas of upper panels in A. White lines indicate the edge of the SVZ. Arrowheads indicate clusters of cells in cKO with progenitor morphology similar to those seen in wild type. (**C-E**) IHC staining of WT and cKO SVZ for Pten (C), NeuN (D) and Dcx (E). The expanded cKO SVZ was deficient for Pten and composed of NeuN+ and Dcx+ cells in contrast to the WT SVZ, which had only thin layers of Dcx+ cells and lacked NeuN+ cells. Lower panels in C and D show higher magnification of the white boxed areas in upper panels. In panel D, the NeuN+ cells adjacent to the WT SVZ were from surrounding striatum and the black line marks the edge of the expanded SVZ in cKO brain. (**F**) Mash1 (white), p-S6 (green) and Dcx (red) triple IF labeling of the expanded cKO SVZ showed a substantial overlap of p-S6+ and Dcx+ cells in the right bottom panel. Scale bars: in A, 50 μm; in B, 10 μm; in C and D upper panels, 50 μm; in C and D lower panels, 10 μm; in E, 50 μm; in F, 20 μm.

RMS (supplementary material Fig. S2) that was most pronounced at the dorsal junction of the SVZ abutting the corpus callosum and the ventral tip where it formed a bulb-like structure. The expansion was easily detectable as early as 20 days post induction (DPI) and was similar at 60, 150, 300 and 540 DPI without progressive enlargement at later time points (data not shown). Close examination of the cell morphology in the SVZ revealed that, in contrast to wild-type control brains in which the SVZ was mainly composed of well-organized spindle-like progenitor cells with scant cytoplasm, the expanded SVZ in *Pten*^{cKO} mice contained a central region of cells with large round nuclei interspersed with isolated progenitor cells, and with clusters of progenitor cells at the edge (Fig. 2B). IHC analysis showed that the expanded SVZ was negative for Pten staining (Fig. 2C) with marked elevation of p-Akt (supplementary material Fig. S3) indicating overall activation of the PI3K pathway in the entire region. When conditional *Pten* deletion was induced in newborn *Pten*^{cKO} mice by TM injection at P0 and P1, similar dorsal SVZ and RMS expansion were consistently detected by P10-30 in the absence of other obvious abnormalities (data not shown), although the ventral expansion of the expanded SVZ was not detected at this age.

The expanded region of the SVZ and RMS was composed of NeuN+ (Rbfox3 – Mouse Genome Informatics) and Dcx+ cells, which mark differentiated neurons and migrating neuroblasts, respectively (Fig. 2D,E; supplementary material Fig. S2B,C). NeuN was not expressed in any of the wild-type SVZ cells, but was strongly expressed in the cKO SVZ, specifically in the cells with larger, rounder nuclei that were not observed in wild-type SVZ (Fig. 2D, lower panel). The expression of Dcx decreased and NeuN expression increased in the ectopic cells as mice aged from 150 to 300 DPI (data not shown). The Dcx+ cells in the expanded SVZ and RMS showed evidence of neuronal differentiation, including abnormal formation of projections (Fig. 2E; supplementary material Fig. S2C). Whereas wild-type Dcx+ neuroblasts did not express p-S6 until reaching the OB (Fig. 1C), Dcx+ neuroblasts of the *Pten*^{cKO} SVZ showed robust p-S6 staining (Fig. 2F), indicating aberrant activation of the PI3K pathway. The ectopic cells also expressed Map2 (Mtap2 – Mouse Genome Informatics) (Fig. 3A,B), a marker of dendrites of differentiated neurons, and calretinin (Calb2 – Mouse Genome Informatics) (Fig. 3C), a marker expressed by mature GABAergic interneurons in the granule cell layer (GCL) and the glomerular cell layer of the OB arising from neuroblasts of the SVZ-RMS (Kohwi et al., 2005; Kohwi et al., 2007; Alvarez-Buylla et al., 2008). This population is the most abundant population of OB neurons produced postnatally. There were also a smaller number of ectopic cells that expressed tyrosine hydroxylase (TH), a marker of dopaminergic interneurons of the glomerular layer, which are less abundant than the calretinin-expressing neurons of the OB (supplementary material Fig. S4) (Batista-Brito et al., 2008). The expression of neuronal markers

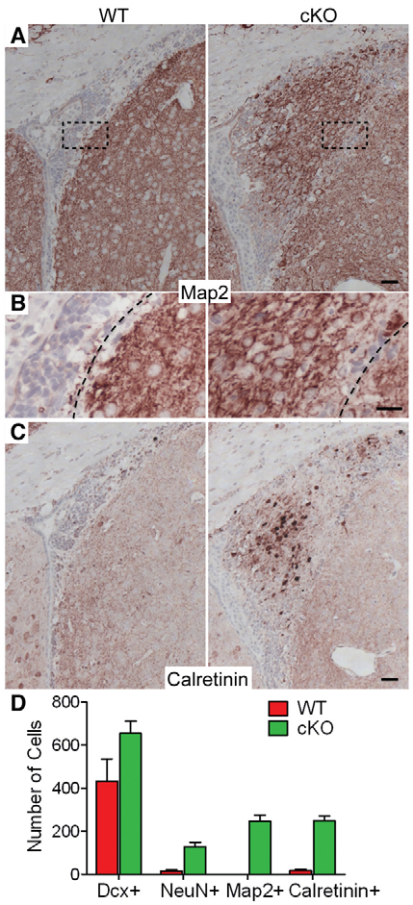

Fig. 3. Ectopic cells in the expanded cKO SVZ expressed markers of mature interneurons of OB. (**A-C**) Map2 (A,B) and calretinin (C) IHC staining of the SVZ from matched coronal brain sections of wild-type (WT) or cKO mice injected with TM at P0-1 and analyzed at P18 showed strong expression of these neuronal differentiation markers in the expanded cKO SVZ that are normally expressed in the OB, but not the SVZ or RMS. B shows higher magnifications of the boxed areas in A. Black dashed lines indicate the edge of the SVZ. (**D**) Quantification of the number of Dcx+, NeuN+, Map2+ and calretinin+ cells in matched sections of the SVZ from mice injected with TM at P11-12 and analyzed at P31. Error bars represent s.e.m. Scale bars: in A,C, 50 μm; in B, 20 μm.

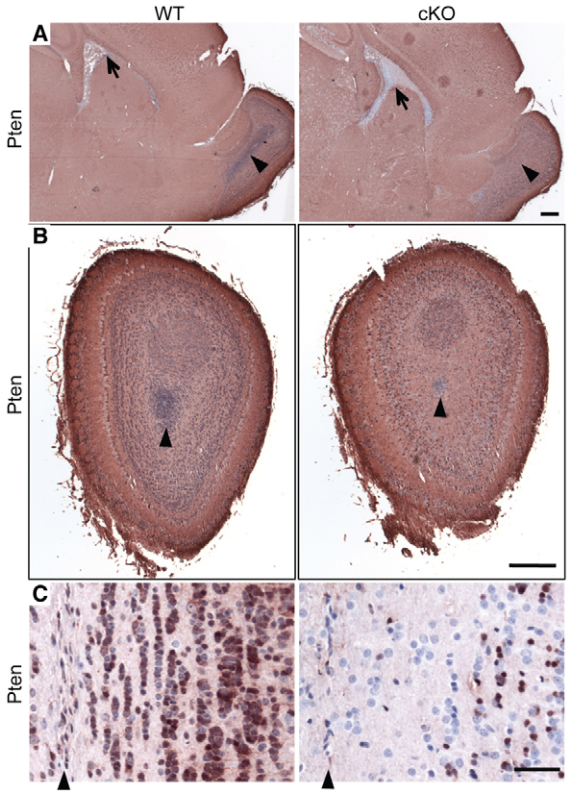

Fig. 4. Reduced diameter of the terminal RMS and decreased granule cell density in the *Pten*^{cKO} OB. (**A-C**) Pten IHC staining from matched sagittal sections of the forebrain (A) or coronal section of the OB (B,C) from wild-type (WT) and cKO mice injected with TM at P0-1 and analyzed at P18 (A,B), or injected with TM at P30-32 and analyzed at 11 months of age (C). The cKO SVZ was expanded and deficient for Pten (A, arrows). The diameter of the terminal RMS in the cKO OB was diminished (B,C, arrowheads). The cell density of the GCL in the cKO OB was reduced (C). Scale bars: in A,B, 300 μm; in C, 50 μm.

of differentiated neurons of the OB in Dcx+ cells in the expanded SVZ indicates ectopic differentiation of neuroblasts that normally remain undifferentiated until they reach the OB. Consistent with a failure of migrating neuroblasts to reach the OB, the diameter of the terminal RMS at the core of the OB and the cell density in the GCL were markedly reduced in *Pten*^{cKO} mice (Fig. 4, Fig. 5A; supplementary material Fig. S5). The ectopic cells expressing neuronal differentiation markers also showed evidence of PI3K/mTorc1 activation as shown by co-expression of Map2 and p-S6 (supplementary material Fig. S6).

Pten loss did not induce substantial changes in proliferation or survival in the expanded *Pten*^{cKO} SVZ

To determine how loss of Pten affected the proliferation in the intact SVZ in vivo, we used both Ki67 IHC and short-term BrdU labeling, which gave consistent results (supplementary material Fig. S7A) (data not shown). The cell numbers in the SVZ of *Pten*^{cKO} mice were increased owing to the presence of ectopic post-mitotic differentiated cells. Considering the percentage of proliferating cells would thus underestimate the proliferation capacity of progenitors in the *Pten*^{cKO} SVZ. Therefore, we counted the absolute numbers of Ki67+ cells from matched SVZs of both wild-type and *Pten*^{cKO} mice. There was no statistically significant difference in proliferation rate in the *Pten*^{cKO} SVZ compared with control littermates (supplementary material Fig. S7A,C).

Activated PI3K signaling can also enhance cell survival; therefore, we used active caspase3 and TUNEL staining to determine whether Pten loss altered apoptosis in the SVZ (supplementary material Fig. S8A). The endogenous level of apoptosis was very low, and not significantly different in wild-type and *Pten*^{cKO} SVZ. Consistent with the resistance of differentiated neurons to radiation-induced death (Frappart and McKinnon, 2008), the expanded portion of the *Pten*^{cKO} SVZ containing differentiated neurons as well as the parenchyma surrounding the SVZ were resistant to irradiation-induced apoptosis (supplementary material Fig. S8B). However, the progenitor cells of both wild type and *Pten*^{cKO} underwent apoptosis 5 hours after exposure to 4 Gy of irradiation. Therefore, Pten-deficient neuroblasts did not show enhanced survival.

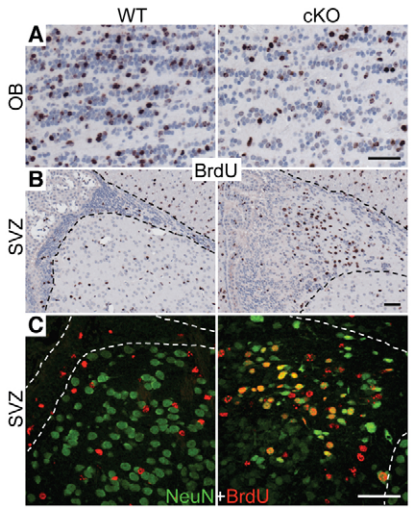

Fig. 5. *Pten*^{cKO} neuroblasts terminated tangential migration prematurely in the SVZ. Immunostaining of matched sagittal sections from wild-type (WT) and cKO mice. Cre activity was induced by TM injection at P0 and P1, BrdU was injected at P4, P5 and P6, and tissue was analyzed at P18. (**A**) In the OB, there were reduced BrdU+ cells in the granule cell layer of the cKO OB compared with WT. (**B**) In the SVZ, there was a significant accumulation of BrdU+ cells in the expanded cKO SVZ. (**C**) BrdU (red) and NeuN (green) double IF labeling of the SVZ from WT and cKO mice showed that a substantial number of BrdU+ cells in the expanded cKO SVZ were NeuN+, whereas there were no NeuN+ cells in the WT SVZ. Black dashed lines in B and white dashed lines in C mark the boundary of the SVZ. Scale bars: 50 μm.

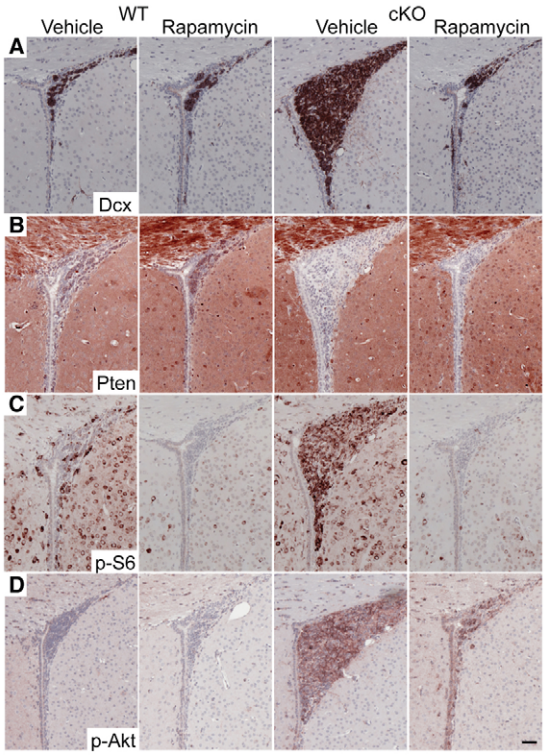

Fig. 6. mTorc1 inhibition rescued the expansion of *Pten*^{cKO} SVZ. (**A-D**) Representative IHC staining for Dcx (A), Pten (B), p-S6 (C) and p-Akt (D) in the SVZ of matched coronal sections from wild-type (WT) or cKO mice. Mice were treated with rapamycin or vehicle from P8 to P31, Cre activity was induced by TM injection at P11 and P12, and tissue was analyzed at P31. Rapamycin completely rescued the enlargement of the cKO SVZ (n=4 in each group). The SVZ of rapamycin-treated cKO mice remained Pten-null (B) and continued to show elevated p-Akt (D), but showed suppression of p-S6 (C), a downstream indicator of mTorc1 activity. Scale bar: 50 μm.

Pten^{cKO} neuroblasts terminated tangential migration prematurely in the SVZ and RMS

To determine whether ectopic neurons arose from proliferative cells in the SVZ that underwent premature termination of migration to the OB, we used BrdU birthdating. *Pten* deletion was induced by TM injection in newborn mice. Four days later, to allow sufficient time for *Pten* deletion and loss of Pten protein, BrdU was injected to label proliferating cells in the SVZ. As expected, the majority of labeled cells in control mice migrated into the GCL of the OB by 15 days after the BrdU pulse (Petreanu and Alvarez-Buylla, 2002) (Fig. 5A). By contrast, there was significant accumulation of BrdU+ cells in the expanded SVZ and greatly reduced numbers of BrdU+ cells, and reduced granule cell density in the OB GCL in the *Pten*^{cKO} mice (Fig. 5A,B; supplementary material Figs S5, S9). A high percentage of BrdU+ cells in the expanded SVZ expressed NeuN, indicating that ectopic differentiated neurons arose from previously proliferating cells in the SVZ (Fig. 5C). In control mice, few BrdU+ cells remained in the SVZ, and none of them expressed NeuN or had the larger rounded morphology seen in ectopic cells in the *Pten*^{cKO} SVZ. They might correspond to slow-cycling neural stem cells or local proliferating glia (Fig. 5C). In the control, BrdU and NeuN double-positive cells were only found in the OB and not in the SVZ or RMS (supplementary material Fig. S9), indicating that BrdU-labeled neuroblasts do not differentiate until they reach the OB in the wild-type mice.

Inhibition of mTorc1 rescued the SVZ-RMS expansion in *Pten*^{cKO} brain

To determine whether inhibition of a downstream effector in the aberrantly activated PI3K pathway could prevent the early termination of tangential migration and ectopic differentiation of *Pten*^{cKO} neuroblasts in the SVZ, we treated the mice with rapamycin, an inhibitor of mTorc1 activity. We previously showed that rapamycin required several days of administration to maximally block mTorc1 signaling in brain (Kwon et al., 2003). Therefore, we pre-treated the mice daily with rapamycin for three days, then induced the deletion of *Pten* with TM at P11-12 and continued rapamycin treatment until P31. Rapamycin treatment completely prevented SVZ expansion in *Pten*^{cKO} mice (Fig. 6A), although the SVZ remained Pten-null in rapamycin-treated mice (Fig. 6B). Rapamycin selectively blocked mTorc1 activity, as shown by lack of p-S6, a downstream indicator of mTorc1 activity (Fig. 6C) without altering levels of p-Akt in the Pten-deficient SVZ (Fig. 6D). Neither apoptosis nor proliferation was affected by rapamycin treatment (supplementary material Fig. S7).

Ex vivo time-lapse live imaging showed *Pten*^{cKO} neuroblasts had normal directional migration with increased speed

To understand how Pten loss affected the movement of tangentially migrating neuroblasts, we used time-lapse live imaging on acute brain slices. We generated *R26LSL-EYFP;Nestin-creER*^{T2}*;Pten*$^{wt/wt}$ (wild type) or *R26LSL-EYFP; Nestin-creER*^{T2}*;Pten*$^{loxP/loxP}$ (*Pten*^{cKO}) mice so that the EYFP cre reporter expression could be used to visualize cells in which cre-mediated recombination occurred. We

induced *Nestin-creER*^{T2} activity at P0 and imaged the RMS in acute brain slices at P16 with two-photon microscopy at the 'elbow' of the RMS, where the RMS curves from ventral towards rostral migration halfway between the SVZ and the OB (see supplementary material Fig. S10A for the location). The majority of visible neuroblasts in the *Pten*^{cKO} brain slices (supplementary material Movie 2) showed directional migration towards the olfactory bulb similar to that observed in wild type (supplementary material Movie 1). However, a small subpopulation of larger cells with rounded morphology that maintained their position were visible in the *Pten*^{cKO}, but not in wild type. Although these movies showed that the directional movement of the majority of *Pten*^{cKO} neuroblasts did not seem to be perturbed, the density of EYFP+ cells was too great to quantify the movement of individual cells. Therefore, we used in vivo electroporation to introduce cre recombinase, allowing visualization of a smaller number of isolated cells that could be reliably tracked over time. We transfected the expression construct *pCAG-Cre* into the SVZ by in vivo electroporation at P2 and visualized transfected cells by expression of the EYFP Cre reporter in *Rosa26-loxP-STOP-loxP-EYFP (R26LSL-EYFP);Pten*$^{wt/wt}$ (wild type) or *R26LSL-EYFP;Pten*$^{loxP/loxP}$ (*Pten*^{cKO}) mice. Neuroblast migration was imaged at P19-20. The majority of EYFP+ cells in the wild-type RMS showed a bipolar morphology, and migrated effectively towards the OB (Fig. 7A,C; supplementary material Movie 3). By contrast, there were two distinct populations of EYFP+ cells in the *Pten*^{cKO} RMS (Fig. 7B; supplementary material Movie 4). One population maintained bipolar morphology and was not significantly different in size or directional migration compared with wild-type control (Fig. 7C-E). Another population lost polarity, showed increased soma size and showed only local non-directional movement. Interestingly, the cells that had stopped directional migration showed active spontaneous membrane ruffling, which distinguished them from completely static cells seen at very low frequency in both the wild-type and *Pten*^{cKO} RMS. The average speed of all EYFP+ cells in the *Pten*^{cKO} RMS (mean: 30.6 μm/hour; n=368), including both cells with normal bipolar morphology and static cells with rounded morphology, was significantly slower than that of the wild type (mean: 47.1 μm/hour; n=194) ($P<10^{-13}$). However, the average speed of bipolar migrating neuroblasts in the *Pten*^{cKO} RMS (mean: 59.2 μm/hour; n=110) was not slower. Indeed, *Pten*^{cKO} neuroblasts that were actively migrating showed a slight increase in speed compared with wild type (mean: 53.8 μm/hour; n=160) (P=0.046) (Fig. 7C). We also measured endpoint speed, a representation of directional movement calculated as the distance between the starting and final position over time. The *Pten*^{cKO} bipolar migrating neuroblasts moved effectively in the appropriate caudal-to-rostral direction, as their endpoint speeds were not significantly different from the wild type (mean 47.6 μm/hour and 44.4 μm/hour, respectively) (P=0.15). Accordingly, a substantial number of Pten-deficient neuroblasts were able to migrate to the OB (supplementary material Fig. S10B,C,E). Both the EYFP+ bipolar and round non-polar cells in the RMS expressed Dcx, indicating that they were migrating neuroblasts or neuroblasts that had stopped migration recently (supplementary material Fig. S10D). These data indicate that Pten deletion does not cause a uniform intrinsic defect that compromises neuroblast directional migration, consistent with premature differentiation resulting in ectopic positioning.

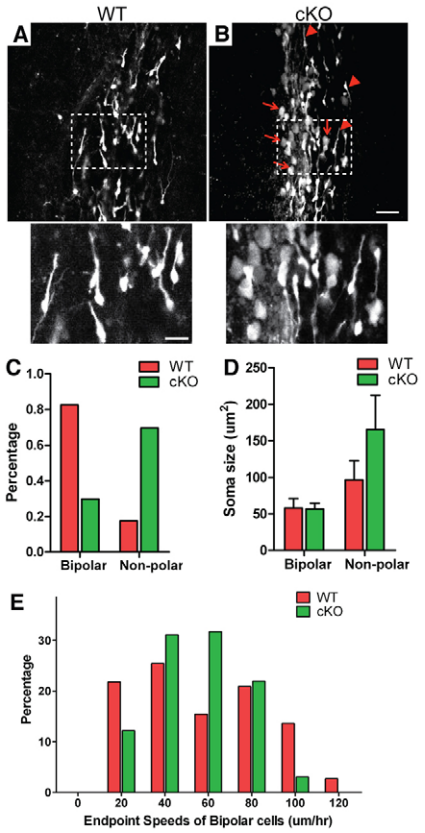

Fig. 7. Ex vivo time-lapse live imaging showed that a subset of *Pten*^{cKO} neuroblasts had normal morphology, size and directional migration. (**A**,**B**) Representative static EYFP images corresponding to time-lapse migration movies from the RMS (supplementary material Movies 3, 4). A Cre expression construct was transfected by in vivo electroporation at P2 into the SVZ of WT (A) or *Pten*$^{flox/flox}$ (cKO) (B) mice carrying the *R26LSL-EYFP* allele. Lower panels are higher magnification of boxed areas in upper panels. Acute brain slices were prepared at P19-20, and cells in which Cre-mediated recombination occurred were visualized by EYFP reporter expression using two-photon microscopy. There were two distinct populations of *Pten*^{cKO} (cKO) neuroblasts: cells with elongated bipolar morphology and normal directional migration (arrowheads) and cells with large rounded morphology that showed only local non-directional movement (arrows). Scale bars: upper panels, 50 μm, lower panels 20 μm. (**C**) Quantification of the percentage of EYFP+ cells with bipolar or non-polar morphology (n=190 for WT and n=368 for cKO). There were significantly more non-polar cells in cKO (green), than in WT (red) (P<0.0001, odds ratio=11). (**D**) The area of EYFP+ somata of non-polar cells was significantly greater in cKO than in WT ($P<10^{-12}$); however, the cells with bipolar morphology were of similar size in cKO and WT (P=0.66). n=22-30 for each morphology. Error bars represent s.e.m. (**E**) Histogram of the endpoint speed, a measure of directional migration, for bipolar migrating EYFP+ cells from WT (red) and cKO RMS (green). n=3 mice per genotype. The average endpoint speed of bipolar migrating neuroblasts in the cKO RMS (mean: 47.6 μm/hour; n=110) was not significantly different from that of WT (mean: 44.4 μm/hour; n=160) (P=0.15).

DISCUSSION

Multiple conditional knockout models have shown that *Pten* deletion during development results in incomplete neuronal migration, disrupting the laminar structure in cerebral cortex and cerebellum. The accumulation of ectopic differentiated *Pten*^{cKO} neurons in the SVZ and RMS observed in the present study is consistent with defects in tangential migration, similar to the failure

of radial glia-guided migration observed in previous models (Backman et al., 2001; Groszer et al., 2001; Kwon et al., 2001; Marino et al., 2002; Yue et al., 2005).

Pten and the PI3K-Akt-mTorc1 pathway have been implicated in cell migration regulation in multiple contexts. Mechanistically, this was mostly clearly demonstrated in *Dictyostelium* where subcellular localization of PTEN and PI3K to the trailing and leading edge of the cell, respectively, established a PIP3 gradient that was required for directional migration and chemotaxis (Funamoto et al., 2002; Iijima and Devreotes, 2002). Deletion of the Akt homolog PkbA, rescued the cytokinesis and chemotaxis defects in PTEN-deficient *Dictyostelium* (Tang et al., 2011). In mammalian cells, the PI3K pathway can regulate cell motility and migration through Akt activation as well as through Akt-independent mechanisms such as Rac1/Cdc42 signaling (Kölsch et al., 2008). In addition, overexpression of wild-type PTEN inhibited migration of human glioma cell lines in an in vitro wound healing assay, and this effect was dependent on the protein phosphatase activity of PTEN independently of PI3K signaling (Raftopoulou et al., 2004).

Unexpectedly, we found that postnatal deletion of *Pten* divided the RMS neuroblasts into two distinct populations: one subset maintained their bipolar morphology and had normal directional migration, and the other population lost polarity and stopped migration. This non-polar morphology, in association with increased frequency of spontaneous protrusions of the plasma membrane, was reminiscent of PTEN-null *Dictyostelium*. However, the population of $Pten^{cKO}$ neuroblasts that maintained bipolar morphology continued moving normally, demonstrating that Pten was not required for directional migration. This is consistent with the observation that some Pten-null cells reach the OB in $Pten^{cKO}$ mice. A previous study in which Pten was deleted in Gfap-expressing neural stem cells also showed that Pten-deficient neurons were capable of reaching the olfactory bulb. This study also noted an expansion of Dcx+ cells in the SVZ and RMS, although they did not analyze expression of mature neuronal markers in these cells (Gregorian et al., 2009). Postnatal deletion of *Pten* in cerebellar granule neurons also showed that a subset of Pten-null granule cells migrated to the proper position in the internal granule layer, whereas many were ectopically located in the molecular layer and at the pial surface (Backman et al., 2001; Kwon et al., 2001). Failed migration of Pten-deficient cerebellar neurons has been suggested to be secondary to defects in the glia guiding their migration (Yue et al., 2005). However, the in vivo electroporation approach used in the present study targeted small numbers of cells and identified stationary Dcx+ neuroblasts without Cre-mediated deletion in surrounding other cell types. Therefore, our results in the RMS are consistent with cell autonomous defects leading to ectopic positioning.

Pten-deficient neuroblasts demonstrated an 'all or none' phenotype of normal directional migration or abnormal morphology associated with arrested migration. The absolute proportion of stationary cells will vary over time as the differentiated cells accumulate, and also die. This dichotomy of phenotypes is distinct from a number of other migration defects that caused an expansion of the SVZ and proximal RMS due to ectopic differentiated neurons. For example, deletion of *Slit1* showed an expansion of the SVZ due to decreased neuroblast migration speed (Kaneko et al., 2010). Live imaging of migrating neuroblasts showed that *Dcx* deletion caused an increase in the number of secondary branches in the leading processes, causing a defect in neuroblast speed, but not in direction of migration (Koizumi et al., 2006). The Pten-deficient phenotype also differs from migration defects caused by mutations in other components of the PI3K pathway. Deletion of *Tsc1* in the neonatal SVZ, which also activates mTorc1, but induces different feedback signaling compared with Pten loss, caused a decrease in neuroblast migration speed (Huang and Manning, 2009; Feliciano and Bordey, 2012). Deletion of *Erbb4*, a receptor tyrosine kinase that has been shown to signal through PI3K as well as other downstream pathways, disrupted proper directional orientation, with a significant decrease in the proportion of neuroblasts migrating towards the OB (Anton et al., 2004).

Normal directional migration of Pten-null neuroblasts is consistent with the finding that directional chemotaxis can still occur in *Dictyostelium* in the absence of a PIP3 gradient (Hoeller and Kay, 2007). Additionally, several studies showed that Pten was not essential in directional migration and chemotaxis of mammalian leukocytes (Lacalle et al., 2004; Ferguson et al., 2007; Nishio et al., 2007; Subramanian et al., 2007; Heit et al., 2008). Pten-deficient neutrophils showed an increased migration speed (Subramanian et al., 2007). Thus, context-dependent signals drive the effect of Pten and PI3K signaling on migration.

Taken together, these data suggest that the ectopic localization of neurons is more likely to be a result of premature differentiation and secondary loss of migration ability rather than intrinsic defects in migration. Indeed, the PI3K-Akt-mTorc1 pathway plays an important role in several crucial neuronal differentiation processes, including neuronal polarity, axon guidance, dendrite arborization and spine morphogenesis (Campbell and Holt, 2001; Jaworski et al., 2005; Kumar et al., 2005; Tavazoie et al., 2005; Chadborn et al., 2006; Kwon et al., 2006; Wildonger et al., 2008; Chow et al., 2009). Direct connections between PI3K signaling and neuronal differentiation were shown in *Drosophila* retina, in which increased insulin receptor/Tor signaling caused precocious differentiation of photoreceptors, and decreased signaling caused delays in differentiation (Bateman and McNeill, 2004). TOR signaling was also required to initiate neuronal differentiation in the chick neural tube (Fishwick et al., 2010).

The PI3K-Akt-mTorc1 pathway is dynamically regulated through the different developmental stages of neuronal lineage along the SVZ-RMS-OB. From birth in the SVZ to differentiation and integration into the local circuit of the OB, neural stem cells progress in phases to transit-amplifying progenitors, migrating neuroblasts and ultimately terminally differentiated mature neurons. Accordingly, cell signaling pathways must be modulated to meet the varying requirements of these differentiation states or to induce transition between consecutive phases. In this study, we found that the PI3K-Akt-mTorc1 pathway is active in the transit-amplifying cells and inactive in the migrating neuroblasts until it is activated again in the OB. Consistent with these findings, previous studies also found high expression of Egfr, a potent PI3K-Akt-mTorc1 pathway activating receptor, in the transit-amplifying progenitors but not in the migrating neuroblasts in the SVZ (Doetsch et al., 2002; Kim et al., 2009; Kokovay et al., 2010). Upregulation of the PI3K-Akt-mTorc1 pathway might act to drive proliferation of transit-amplifying progenitors, whereas inactivation of PI3K-Akt-mTorc1 signaling through Pten expression might play a role in the transition to migrating neuroblasts that exit the cell cycle. The proliferation consequences downstream of Pten loss are likely to be influenced by the extent of upstream activation of PI3K driven by the growth factor environment at different developmental stages.

In wild-type RMS, the PI3K-Akt-mTorc1 pathway is not activated in Dcx+ cells until they reach the OB, correlating well with the time at which they begin further differentiation. This

suggests that the PI3K-Akt-mTorc1 pathway might be involved in the transition from a migratory neuroblast to a differentiating neuron in response to local environmental cues. In the absence of Pten, premature activation of PI3K signaling in neuroblasts in the RMS probably triggers precocious differentiation resulting in ectopic positioning. Inhibition of mTorc1 activity effectively rescued ectopic differentiation of neuroblasts and prevented the expansion of the SVZ and RMS. mTorc1 modulates protein synthesis and cell growth and plays an important role in neuronal differentiation processes (Campbell and Holt, 2001; Jaworski et al., 2005; Kumar et al., 2005; Tavazoie et al., 2005; Kwon et al., 2006; Wildonger et al., 2008; Chow et al., 2009). Taken together, our results, along with previous studies, suggest that proper temporal and spatial regulation of the PI3K-Akt-mTorc1 pathway plays an important role in regulating the appropriate timing and positioning for neuronal differentiation, but is not required for directional tangential neuronal migration.

Acknowledgements
We thank J. Mitchell and K. Cox for genotyping the St Jude Transgenic Core Facility for expertise in generating *Nestin-creER^{T2}* mice; and the St Jude Cell and Tissue Imaging Shared Resource for confocal microscopy. We thank Tak Mak (University of Toronto) for providing *Pten^{loxP}* mice and Pierre Chambon (IGBMC) for *Nestin-creER^{T2}* cDNA.

Funding
L.M.L.C. was supported by the Jean-François St-Denis Fellowship in Cancer Research from the Canadian Institutes of Health Research. This work was supported by National Institutes of Health (NIH) grants [CA096832 and CA135554 to S.J.B.]; the Cancer Center Core grant [CA21765]; and by American Lebanese Syrian Associated Charities (ALSAC). Deposited in PMC for release after 12 months.

Competing interests statement
The authors declare no competing financial interests.

Supplementary material
Supplementary material available online at
http://dev.biologists.org/lookup/suppl/doi:10.1242/dev.083154/-/DC1

References

Alvarez-Buylla, A. and Garcia-Verdugo, J. M. (2002). Neurogenesis in adult subventricular zone. *J. Neurosci.* **22**, 629-634.
Alvarez-Buylla, A., Kohwi, M., Nguyen, T. M. and Merkle, F. T. (2008). The heterogeneity of adult neural stem cells and the emerging complexity of their niche. *Cold Spring Harb. Symp. Quant. Biol.* **73**, 357-365.
Anton, E. S., Ghashghaei, H. T., Weber, J. L., McCann, C., Fischer, T. M., Cheung, I. D., Gassmann, M., Messing, A., Klein, R., Schwab, M. H. et al. (2004). Receptor tyrosine kinase ErbB4 modulates neuroblast migration and placement in the adult forebrain. *Nat. Neurosci.* **7**, 1319-1328.
Backman, S. A., Stambolic, V., Suzuki, A., Haight, J., Elia, A., Pretorius, J., Tsao, M. S., Shannon, P., Bolon, B., Ivy, G. O. et al. (2001). Deletion of Pten in mouse brain causes seizures, ataxia and defects in soma size resembling Lhermitte-Duclos disease. *Nat. Genet.* **29**, 396-403.
Bateman, J. M. and McNeill, H. (2004). Temporal control of differentiation by the insulin receptor/tor pathway in Drosophila. *Cell* **119**, 87-96.
Batista-Brito, R., Close, J., Machold, R. and Fishell, G. (2008). The distinct temporal origins of olfactory bulb interneuron subtypes. *J. Neurosci.* **28**, 3966-3975.
Boutin, C., Diestel, S., Desoeuvre, A., Tiveron, M. C. and Cremer, H. (2008). Efficient in vivo electroporation of the postnatal rodent forebrain. *PLoS ONE* **3,** e1883.
Cain, R. J. and Ridley, A. J. (2009). Phosphoinositide 3-kinases in cell migration. *Biol. Cell* **101**, 13-29.
Campbell, D. S. and Holt, C. E. (2001). Chemotropic responses of retinal growth cones mediated by rapid local protein synthesis and degradation. *Neuron* **32**, 1013-1026.
Chadborn, N. H., Ahmed, A. I., Holt, M. R., Prinjha, R., Dunn, G. A., Jones, G. E. and Eickholt, B. J. (2006). PTEN couples Sema3A signalling to growth cone collapse. *J. Cell Sci.* **119**, 951-957.
Chalhoub, N. and Baker, S. J. (2009). PTEN and the PI3-kinase pathway in cancer. *Annu. Rev. Pathol.* **4**, 127-150.
Chesler, A. T., Le Pichon, C. E., Brann, J. H., Araneda, R. C., Zou, D. J. and Firestein, S. (2008). Selective gene expression by postnatal electroporation during olfactory interneuron neurogenesis. *PLoS ONE* **3**, e1517.
Chow, D. K., Groszer, M., Pribadi, M., Machniki, M., Carmichael, S. T., Liu, X. and Trachtenberg, J. T. (2009). Laminar and compartmental regulation of dendritic growth in mature cortex. *Nat. Neurosci.* **12**, 116-118.
Chow, L. M., Zhang, J. and Baker, S. J. (2008). Inducible Cre recombinase activity in mouse mature astrocytes and adult neural precursor cells. *Transgenic Res.* **17**, 919-928.
Cicero, S. A., Johnson, D., Reyntjens, S., Frase, S., Connell, S., Chow, L. M., Baker, S. J., Sorrentino, B. P. and Dyer, M. A. (2009). Cells previously identified as retinal stem cells are pigmented ciliary epithelial cells. *Proc. Natl. Acad. Sci. USA* **106**, 6685-6690.
Doetsch, F., Petreanu, L., Caille, I., Garcia-Verdugo, J. M. and Alvarez-Buylla, A. (2002). EGF converts transit-amplifying neurogenic precursors in the adult brain into multipotent stem cells. *Neuron* **36**, 1021-1034.
Endersby, R. and Baker, S. J. (2008). PTEN signaling in brain: neuropathology and tumorigenesis. *Oncogene* **27**, 5416-5430.
Engelman, J. A., Luo, J. and Cantley, L. C. (2006). The evolution of phosphatidylinositol 3-kinases as regulators of growth and metabolism. *Nat. Rev. Genet.* **7**, 606-619.
Feil, R., Brocard, J., Mascrez, B., LeMeur, M., Metzger, D. and Chambon, P. (1996). Ligand-activated site-specific recombination in mice. *Proc. Natl. Acad. Sci. USA* **93**, 10887-10890.
Feil, R., Wagner, J., Metzger, D. and Chambon, P. (1997). Regulation of Cre recombinase activity by mutated estrogen receptor ligand-binding domains. *Biochem. Biophys. Res. Commun.* **237**, 752-757.
Feliciano, D. and Bordey, A. (2012). Postnatal neurogenesis generates heterotopias, olfactory micronodules and cortical infiltration following single-cell Tsc1 deletion. *Human Mol. Genet.* **21**, 799-810.
Ferguson, G. J., Milne, L., Kulkarni, S., Sasaki, T., Walker, S., Andrews, S., Crabbe, T., Finan, P., Jones, G., Jackson, S. et al. (2007). PI(3)Kgamma has an important context-dependent role in neutrophil chemokinesis. *Nat. Cell Biol.* **9**, 86-91.
Fishwick, K. J., Li, R. A., Halley, P., Deng, P. and Storey, K. G. (2010). Initiation of neuronal differentiation requires PI3-kinase/TOR signalling in the vertebrate neural tube. *Dev. Biol.* **338**, 215-225.
Frappart, P. O. and McKinnon, P. J. (2008). Mouse models of DNA double-strand break repair and neurological disease. *DNA Repair (Amst.)* **7**, 1051-1060.
Funamoto, S., Meili, R., Lee, S., Parry, L. and Firtel, R. A. (2002). Spatial and temporal regulation of 3-phosphoinositides by PI 3-kinase and PTEN mediates chemotaxis. *Cell* **109**, 611-623.
Ghashghaei, H. T., Lai, C. and Anton, E. S. (2007). Neuronal migration in the adult brain: are we there yet? *Nat. Rev. Neurosci.* **8**, 141-151.
Gregorian, C., Nakashima, J., Le Belle, J., Ohab, J., Kim, R., Liu, A., Smith, K. B., Groszer, M., Garcia, A. D., Sofroniew, M. V. et al. (2009). Pten deletion in adult neural stem/progenitor cells enhances constitutive neurogenesis. *J. Neurosci.* **29**, 1874-1886.
Groszer, M., Erickson, R., Scripture-Adams, D. D., Lesche, R., Trumpp, A., Zack, J. A., Kornblum, H. I., Liu, X. and Wu, H. (2001). Negative regulation of neural stem/progenitor cell proliferation by the Pten tumor suppressor gene in vivo. *Science* **294**, 2186-2189.
Heit, B., Robbins, S. M., Downey, C. M., Guan, Z., Colarusso, P., Miller, B. J., Jirik, F. R. and Kubes, P. (2008). PTEN functions to 'prioritize' chemotactic cues and prevent 'distraction' in migrating neutrophils. *Nat. Immunol.* **9**, 743-752.
Hoeller, O. and Kay, R. R. (2007). Chemotaxis in the absence of PIP3 gradients. *Curr. Biol.* **17**, 813-817.
Huang, J. and Manning, B. D. (2009). A complex interplay between Akt, TSC2 and the two mTOR complexes. *Biochem. Soc. Trans.* **37**, 217-222.
Iijima, M. and Devreotes, P. (2002). Tumor suppressor PTEN mediates sensing of chemoattractant gradients. *Cell* **109**, 599-610.
Inoki, K., Corradetti, M. N. and Guan, K. L. (2005). Dysregulation of the TSC-mTOR pathway in human disease. *Nat. Genet.* **37**, 19-24.
Jaworski, J., Spangler, S., Seeburg, D. P., Hoogenraad, C. C. and Sheng, M. (2005). Control of dendritic arborization by the phosphoinositide-3'-kinase-Akt-mammalian target of rapamycin pathway. *J. Neurosci.* **25**, 11300-11312.
Kaneko, N., Marín, O., Koike, M., Hirota, Y., Uchiyama, Y., Wu, J. Y., Lu, Q., Tessier-Lavigne, M., Alvarez-Buylla, A., Okano, H. et al. (2010). New neurons clear the path of astrocytic processes for their rapid migration in the adult brain. *Neuron* **67**, 213-223.
Kim, Y., Comte, I., Szabo, G., Hockberger, P. and Szele, F. G. (2009). Adult mouse subventricular zone stem and progenitor cells are sessile and epidermal growth factor receptor negatively regulates neuroblast migration. *PLoS ONE* **4**, e8122.
Kirschenbaum, B., Doetsch, F., Lois, C. and Alvarez-Buylla, A. (1999). Adult subventricular zone neuronal precursors continue to proliferate and migrate in the absence of the olfactory bulb. *J. Neurosci.* **19**, 2171-2180.
Kohwi, M., Osumi, N., Rubenstein, J. L. and Alvarez-Buylla, A. (2005). Pax6 is required for making specific subpopulations of granule and periglomerular neurons in the olfactory bulb. *J. Neurosci.* **25**, 6997-7003.

Kohwi, M., Petryniak, M. A., Long, J. E., Ekker, M., Obata, K., Yanagawa, Y., Rubenstein, J. L. and Alvarez-Buylla, A. (2007). A subpopulation of olfactory bulb GABAergic interneurons is derived from Emx1- and Dlx5/6-expressing progenitors. *J. Neurosci.* **27**, 6878-6891.
Koizumi, H., Tanaka, T. and Gleeson, J. G. (2006). Doublecortin-like kinase functions with doublecortin to mediate fiber tract decussation and neuronal migration. *Neuron* **49**, 55-66.
Kokovay, E., Goderie, S., Wang, Y., Lotz, S., Lin, G., Sun, Y., Roysam, B., Shen, Q. and Temple, S. (2010). Adult SVZ lineage cells home to and leave the vascular niche via differential responses to SDF1/CXCR4 signaling. *Cell Stem Cell* **7**, 163-173.
Kölsch, V., Charest, P. G. and Firtel, R. A. (2008). The regulation of cell motility and chemotaxis by phospholipid signaling. *J. Cell Sci.* **121**, 551-559.
Kumar, V., Zhang, M. X., Swank, M. W., Kunz, J. and Wu, G. Y. (2005). Regulation of dendritic morphogenesis by Ras-PI3K-Akt-mTOR and Ras-MAPK signaling pathways. *J. Neurosci.* **25**, 11288-11299.
Kwon, C. H., Zhu, X., Zhang, J., Knoop, L. L., Tharp, R., Smeyne, R. J., Eberhart, C. G., Burger, P. C. and Baker, S. J. (2001). Pten regulates neuronal soma size: a mouse model of Lhermitte-Duclos disease. *Nat. Genet.* **29**, 404-411.
Kwon, C. H., Zhu, X., Zhang, J. and Baker, S. J. (2003). mTor is required for hypertrophy of Pten-deficient neuronal soma in vivo. *Proc. Natl. Acad. Sci. USA* **100**, 12923-12928.
Kwon, C. H., Luikart, B. W., Powell, C. M., Zhou, J., Matheny, S. A., Zhang, W., Li, Y., Baker, S. J. and Parada, L. F. (2006). Pten regulates neuronal arborization and social interaction in mice. *Neuron* **50**, 377-388.
Lacalle, R. A., Gómez-Moutón, C., Barber, D. F., Jiménez-Baranda, S., Mira, E., Martínez-A., C., Carrera, A. C. and Mañes, S. (2004). PTEN regulates motility but not directionality during leukocyte chemotaxis. *J. Cell Sci.* **117**, 6207-6215.
Marino, S., Krimpenfort, P., Leung, C., van der Korput, H. A., Trapman, J., Camenisch, I., Berns, A. and Brandner, S. (2002). PTEN is essential for cell migration but not for fate determination and tumourigenesis in the cerebellum. *Development* **129**, 3513-3522.
Metzger, D., Clifford, J., Chiba, H. and Chambon, P. (1995). Conditional site-specific recombination in mammalian cells using a ligand-dependent chimeric Cre recombinase. *Proc. Natl. Acad. Sci. USA* **92**, 6991-6995.
Nishio, M., Watanabe, K., Sasaki, J., Taya, C., Takasuga, S., Iizuka, R., Balla, T., Yamazaki, M., Watanabe, H., Itoh, R. et al. (2007). Control of cell polarity and motility by the PtdIns(3,4,5)P3 phosphatase SHIP1. *Nat. Cell Biol.* **9**, 36-44.
Petreanu, L. and Alvarez-Buylla, A. (2002). Maturation and death of adult-born olfactory bulb granule neurons: role of olfaction. *J. Neurosci.* **22**, 6106-6113.
Polleux, F. and Ghosh, A. (2002). The slice overlay assay: a versatile tool to study the influence of extracellular signals on neuronal development. *Sci. STKE* **2002**, pl9.
Raftopoulou, M., Etienne-Manneville, S., Self, A., Nicholls, S. and Hall, A. (2004). Regulation of cell migration by the C2 domain of the tumor suppressor PTEN. *Science* **303**, 1179-1181.
Snapyan, M., Lemasson, M., Brill, M. S., Blais, M., Massouh, M., Ninkovic, J., Gravel, C., Berthod, F., Götz, M., Barker, P. A. et al. (2009). Vasculature guides migrating neuronal precursors in the adult mammalian forebrain via brain-derived neurotrophic factor signaling. *J. Neurosci.* **29**, 4172-4188.
Soriano, P. (1999). Generalized lacZ expression with the ROSA26 Cre reporter strain. *Nat. Genet.* **21**, 70-71.
Srinivas, S., Watanabe, T., Lin, C. S., William, C. M., Tanabe, Y., Jessell, T. M. and Costantini, F. (2001). Cre reporter strains produced by targeted insertion of EYFP and ECFP into the ROSA26 locus. *BMC Dev. Biol.* **1**, 4.
Subramanian, K. K., Jia, Y., Zhu, D., Simms, B. T., Jo, H., Hattori, H., You, J., Mizgerd, J. P. and Luo, H. R. (2007). Tumor suppressor PTEN is a physiologic suppressor of chemoattractant-mediated neutrophil functions. *Blood* **109**, 4028-4037.
Suzuki, A., Yamaguchi, M. T., Ohteki, T., Sasaki, T., Kaisho, T., Kimura, Y., Yoshida, R., Wakeham, A., Higuchi, T., Fukumoto, M. et al. (2001). T cell-specific loss of Pten leads to defects in central and peripheral tolerance. *Immunity* **14**, 523-534.
Tang, M., Iijima, M., Kamimura, Y., Chen, L., Long, Y. and Devreotes, P. (2011). Disruption of PKB signaling restores polarity to cells lacking tumor suppressor PTEN. *Mol. Biol. Cell* **22**, 437-447.
Tavazoie, S. F., Alvarez, V. A., Ridenour, D. A., Kwiatkowski, D. J. and Sabatini, B. L. (2005). Regulation of neuronal morphology and function by the tumor suppressors Tsc1 and Tsc2. *Nat. Neurosci.* **8**, 1727-1734.
Waite, K. and Eickholt, B. J. (2010). The neurodevelopmental implications of PI3K signaling. *Curr. Top. Microbiol. Immunol.* **346**, 245-265.
Wildonger, J., Jan, L. Y. and Jan, Y. N. (2008). The Tsc1-Tsc2 complex influences neuronal polarity by modulating TORC1 activity and SAD levels. *Genes Dev.* **22**, 2447-2453.
Yue, Q., Groszer, M., Gil, J. S., Berk, A. J., Messing, A., Wu, H. and Liu, X. (2005). PTEN deletion in Bergmann glia leads to premature differentiation and affects laminar organization. *Development* **132**, 3281-3291.
Zimmerman, L., Lendahl, U., Cunningham, M., McKay, R., Parr, B., Gavin, B., Mann, J., Vassileva, G. and McMahon, A. (1994). Independent regulatory elements in the nestin gene direct transgene expression to neural stem cells or muscle precursors. *Neuron* **12**, 11-24.